Chemical Engineering Journal 96 (2003) 3–13

Chemical Engineering Journal

www.elsevier.com/locate/cej

CFD modelling and experimental validation of particle-to-fluid mass and heat transfer in a packed bed at very low channel to particle diameter ratio

S.J.P. Romkes [a], F.M. Dautzenberg [b], C.M. van den Bleek [a], H.P.A. Calis [a,*]

[a] *Faculty of Applied Sciences, Delft University of Technology, DelftChemTech, Julianalaan 136, 2628 BL Delft, The Netherlands*
[b] *Technology Development Center, ABB Lummus Global Inc., 1515 Broad Street, Bloomfield, NJ, USA*

Abstract

In this paper, the mass and heat transfer characteristics of a composite structured catalytic reactor packing (Composite Structured Packing (CSP)) are investigated. A CSP consists of a multichannel framework filled with ordinary catalyst particles, with a square channel-to-particle-diameter ratio (N) of $1 < N < 5$, resulting in a system with a significantly lower pressure drop compared to a randomly packed bed. The goal of the present study is to assess whether commercial Computational Fluid Dynamics (CFD) software can be used to (1) adequately predict the rate of mass and heat transfer from the catalyst particles to the fluid in a CSP and (2) develop simple engineering correlations for this type of packing. First, it is shown that commercial CFD software (CFX-5.3) can be used to adequately predict the particle-to-fluid heat transfer of a single free sphere. Furthermore, it is shown that the CFD code can predict the heat/mass transfer characteristics, with an average error of 15% compared to experimental values, for packed beds of spherical particles with $1.00 \leqslant N \leqslant 2.00$. The constants of the commonly used engineering correlation $Nu = c_1 + c_2 Re^n Pr^{1/3}$ were obtained by fitting the CFD results for $N = 1.00$, 1.15, 1.47, 2.00A and 2.00B.

Keywords: Computational Fluid Dynamics; Packed bed reactor; Structured packing; Mass and heat transfer; Low channel-to-particle-diameter ratio

1. Introduction

In industrial applications, catalysts are used to enhance chemical reactions. Very often, the catalysts are applied in wide, randomly packed (fixed) beds, which are not necessarily the most favourable or most efficient packing. Although not optimal, random packings will probably remain the standard for catalytic reactors for some decades because of their low cost and ease of use compared to structured packings. Because of low pressure drop requirements or other specific demands in chemical processes, the development and application of novel structured packings and reactors, has been increasing over the last decades. The reactor engineering characteristics of these packings and reactors, such as pressure drop, channelling and bypassing behaviour, dispersion and mass and heat transfer, have to be known, and simple engineering (design) correlations should be available.

The modelling of the characteristics of packed beds is mostly done with models that are based on physical principles, and contain parameters that have been determined in laboratory experiments. Computer speed has increased tremendously over the last few years. It becomes interesting, tempting and within acceptable time and cost constraints to simulate (parts of) structured catalyst beds with 3D Computational Fluid Dynamics (CFD), in order to predict the reactor engineering characteristics and to provide insight in flow patterns from macro to micro scale sizes. The main advantage of this approach is that a number of configurations of structures of packings and/or reactors can be evaluated without the construction of, and investment in, experimental apparatus. Also a higher flexibility in settings in experimental set-ups, such as adiabatic experiments or experiments at very low or high Reynolds numbers, is achievable.

In this paper, this modelling approach is applied to a novel structured catalytic reactor packing, called a Composite Structured Packing (CSP [18]), that enables the use of ordinary catalyst particles in a fixed bed, at significantly lower pressure drops compared to a randomly packed bed. The CSP concept is based on the well-known principle that in a randomly packed bed, the presence of the wall induces an ordering of the particles, accompanied by a higher voidage and lower tortuosity. This principle can be exploited

* Corresponding author. Tel.: +31-15-278-3516; fax: +31-15-278-4452.
E-mail address: h.p.calis@tnw.tudelft.nl (H.P.A. Calis).
URL: http://www.dct.tudelft.nl/race/index_ie.html.

1385-8947/$ – see front matter © 2003 Elsevier B.V. All rights reserved.
doi:10.1016/j.cej.2003.08.026

Nomenclature

A	surface area (m^2)
c_1, c_2	constant in correlation
c_p	heat capacity ($J\,kg^{-1}\,K^{-1}$)
C	concentration ($mol_A\,m_{gas}^{-3}$)
d	diameter (m)
D	molecular diffusion coefficient ($m^2\,s^{-2}$)
h	heat transfer coefficient ($W\,m^{-2}\,K$)
j	Chilton–Colburn j factor
k_g	gas phase mass transfer coefficient ($m\,s^{-1}$)
m	mass (kg)
M	molar mass of naphthalene ($g\,mol^{-1}$)
n	number of moles (mol), exponent
N	channel-to-particle-diameter ratio ($m\,m^{-1}$)
p	number of mass transfer experiments at a specific Reynolds number
P	pressure (Pa)
q	heat transfer rate ($kg\,s^{-1}$)
q''	heat flux ($kg\,m^{-2}\,s^{-1}$)
R	ideal gas constant, 8.3144 ($J\,mol^{-1}\,K^{-1}$)
t	time (s)
T	temperature (K)
v	velocity ($m\,s^{-1}$)
V	volume (m^3)
x	number of mass transfer experiments at different Reynolds numbers

Greek letters

ϵ	porosity ($m_{gas}^3\,m_{reactor}^{-3}$)
φ	total transfer rate ($mol\,s^{-1}$)
λ	thermal conductivity ($W\,m^{-1}\,K$)
μ	dynamic viscosity (Pa s)
ν	kinematic viscosity (Pa s)

Subscripts

bulk	in the bulk phase
D	analogy letter for mass transfer (referring to diffusion)
gas	of the gas phase
H	hydraulic, analogy letter for heat transfer
i	interstitial
in	at the inlet
m	mass
mol	molar
out	at the outlet
p	particle
s	solid, surface or superficial
sat	saturated
w	heat, at the wall

Dimensionless groups

Nu	$\equiv \frac{hd}{\lambda}$
Pr	$\equiv \frac{\mu c_p}{\lambda}$
Re	$\equiv \frac{\rho v d}{\mu}$
Sc	$\equiv \frac{\mu}{\rho D}$
Sh	$\equiv \frac{k_g d}{D}$

by filling an array of parallel channels, such as a monolith or honeycomb, with ordinary catalyst particles (see Fig. 1).

The CSP can create a significantly lower pressure drop (up to a factor 15) per unit catalyst mass than a randomly packed bed containing the same catalyst particles, as has been shown in our previous paper [4]. Alternatively, the CSP concept allows the use of smaller particles, yet at the same pressure drop as across a randomly packed bed, favouring the catalyst efficiency and selectivity. However, the analogy between momentum transfer and mass and heat transfer predicts that if the pressure drop is lower, also the rate of mass and heat transfer between fluid and solids will be lower, compared to a traditional ($N > 10$) randomly packed bed. Hence, mass and heat transfer in a CSP will be more critical than in a traditional fixed bed.

In the modelling of ΔP and particle-to-fluid mass and heat transfer, all CSP channels can be assumed to behave identically. Thus, modelling of a CSP is reduced to the modelling of single fixed beds with a very low channel-to-particle diameter ratio N. Transport phenomena in fixed beds with $N < 4.0$ have relatively little been studied, and relations to predict these properties are scarce. Tsotsas and Schlünder [20] have measured the mass transfer rates of naphthalene particles to air at low tube-to-particle-diameter ratios of 1.41, 1.98 and 3.77, and calculated the corresponding Sherwood numbers via the axially dispersed plug flow model. The results were compared with predictions according to the correlation of Gnielinski [9] (accounting for porosity), and Wakao and Funazkri [22] (not accounting for porosity), originally developed for wide packed beds. Their main conclusion is that these relations overestimate the mass transfer extensively (40 and 50–110%, respectively), especially at low Reynolds numbers. Winterberg and Tsotas [24,25] developed a model to describe the effective radial heat conductivity in packed beds of a low channel-to-particle-diameter ratio and extended their model for packings of spheres to cylinders. It has been successfully compared with various bed

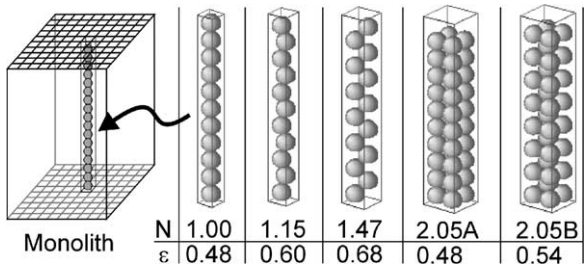

Fig. 1. Concept of Composite Structured Packing (CSP) and simulated packings with their aspect ratios (N) and porosity (ϵ).

geometries, and several different boundary conditions. Winterberg and Tsotsas [26] also review earlier work, investigating the issue of pressure drop in spatially constrained packed beds.

In general, 2D and 3D CFD models have been used in various fields to simulate flow profiles and heat transfer. Using the 2D finite elements method, Dalman et al. [5] investigated the flow around two spheres near a wall in an axisymmetric plane. The formation of eddies between the spheres, leading to regions of poor heat transfer, has been shown in this work. Lloyd and Boehm [14] studied a linear array of eight spheres in 2D, to determine the influence of the sphere spacing on the drag coefficients and the particle-to-fluid heat transfer. It was shown that a decreasing space between the spheres resulted in a decreased heat transfer.

More recently, 3D models of packed beds have been developed. Derkx and Dixon [6] developed a simple model consisting of three spheres in a tube, in order to investigate the wall heat transfer coefficients. Logtenberg and Dixon [11,12] extended this model to eight spheres, divided in two layers of four spheres without solid–solid contact points. Logtenberg et al. [13] however, incorporated contact points between the solids in a ten-sphere model, which used spherical dead volumes around the contact points. This model showed flow and heat transfer behaviour that could not be described by conventional fixed bed models.

Recently, Nijemeisland and Dixon [16] modelled the channel wall-to-fluid heat transfer in packed beds for circular tubes with low channel-to-particle-diameter ratios, using CFD. They presented an extensive overview of previous work on modelling and measurement of the characteristics of fixed beds with low channel-to-particle-diameter ratios. Correction factors for non-ideal experimental measurement and omitted heat transfer mechanisms in the CFD model were introduced. After correction, the wall-to-fluid heat transfer simulations in a CFD model geometry, consisting of 44 solid spheres in a tube of $N = 2.00$, showed a very good quantitative and qualitative fit to experimentally measured temperature profiles of the same geometry.

We showed earlier [4] that commercial CFD software (CFX-5.2) can be used to adequately predict pressure drop characteristics and local fluid velocities in a CSP. Nijemeisland and Dixon [16] showed the capability of CFD to predict temperature profiles induced by the channel wall-to-fluid heat transfer in models of a single tube filled with spherical particles.

The objective of this work is (1) to assess whether commercial CFD software (CFX-5.3) can be used to predict the rate of the mass and heat transfer from the catalyst particles to the fluid in a CSP (expressed as Nusselt versus Reynolds) within a target error of 20% and (2) whether it can be used to develop (simple) engineering correlations for this type of packing. The CFD simulation of heat transfer will be validated by comparing the data with experimentally determined particle-to-fluid mass transfer rates (expressed as Sherwood versus Reynolds), by making use of Chilton–Colburn analogy between mass and heat transfer.

The following approach is followed. First, a benchmark is performed to assess the heat transfer simulation capabilities of the CFD code. In this benchmark, the particle-to-fluid heat transfer of a single sphere in an 'infinite' domain is simulated. Although this is a standard case, it has relatively little been studied in literature, which is a reason to describe it here. The simulation results will be compared to theoretical and experimental data in existing literature in order to validate the use of the simulation method and software. Second, particle-to-fluid heat transfer simulations are performed for the CSPs with channel-to-particle-diameter ratios as shown in Fig. 1. Various analyses of the influence on the calculated heat transfer or Nusselt number will be performed, such as the grid size dependency, the so-called 'shrink' factor (to prevent mesh problems because of contact points between solids, Calis et al. [4], or 'near-miss' model by Nijemeisland and Dixon [16]) and the number and position of the heated particles. In parallel, naphthalene sublimation mass transfer experiments are carried out to obtain the corresponding Sherwood numbers, which under present conditions can safely be assumed to be identical to the Nusselt numbers. Finally, engineering correlations, based on the Nusselt numbers from the heat transfer simulations, will be developed and validated by comparison with the experimental Sherwood numbers by using the mass and heat transfer analogy.

2. Basic considerations

2.1. Engineering practice in mass/heat transfer modelling

The Nusselt (Sherwood) number that quantifies heat (mass) transfer from a surface to a fluid is a function of the Reynolds and Prandtl (Schmidt) number. This is generalized into correlations of the form:

$$Nu = c_1 + c_2 Re^n Pr^{1/3} \quad (1)$$

$$Sh = c_1 + c_2 Re^n Sc^{1/3} \quad (2)$$

Although these equations seem simple, a stagnant, laminar or turbulent flow situation has a complete different background in this relation. This is important in the simulation of particle-to-fluid heat transfer. Therefore, the heat transfer (expressed as the Nusselt number) for six special cases will be discussed: (1) the particle-to-fluid heat transfer of a single free sphere in a static infinite medium, (2) the particle-to-fluid heat transfer of a single free sphere in a flowing fluid, (3) the wall-to-fluid heat transfer of an empty channel without flow, (4) the wall-to-fluid heat transfer of an empty channel with laminar flow, (5) the wall-to-fluid heat transfer of an empty channel with turbulent flow, and (6) the particle-to-fluid heat transfer of a tube filled with catalyst particles. In the steady state situation of case (1), heat is still transferred from the particle to the infinite domain

which has a constant bulk temperature infinitely far away. Theoretically, it can be derived that $Nu = 2$ in this case [3]. For case (2), the Nusselt number increases with increasing Reynolds number, according to Eq. (1). In the steady state situation of case (3), the Nusselt number cannot be defined because the fluid in the channel has attained the wall temperature, thus no temperature gradient exists anymore. Depending on the channel shape and the boundary condition in case (4), where the radial temperature profile is not a function of Reynolds, $Nu = 3.66$ for an empty cylindrical tube under a constant temperature boundary condition, whereas $Nu = 4.36$ under a constant heat flux boundary condition. For turbulent flow in case (5), the radial temperature profile becomes a function of Reynolds and again Nusselt increases with Reynolds, according to Eq. (1). Finally, in case (6) the fluid flow path and heat flux are yet again constrained in the radial direction as was for the empty tube, which results in a similar dependence of Nusselt on Reynolds as in case (4) and case (5): constant Nusselt number for laminar flow and Reynolds dependent for turbulent flow.

The conclusion of these six cases is that, both for a single free sphere and for an empty channel or tube filled with particles, a limiting value of Nusselt exists, and dependence of Nusselt on Reynolds is described by Eq. (1). However, for a single free sphere the limiting value is obtained at $Re = 0$, and Nusselt increases with Reynolds both at laminar and turbulent flow, whereas for an empty channel or a tube filled with particles, Nusselt is undefined at $Re = 0$, Nusselt is constant at laminar flow, whereas Nusselt depends on Reynolds in the transition regime or at turbulent flow.

In this paper, the particle-to-fluid heat transfer rate, q (W), from a sphere to a fluid is simulated with CFD. The temperature of the surface of the particle is set to a surface temperature, T_s, whereas the fluid at the boundary of the domain is set to a lower bulk temperature, T_∞. As a result of the temperature difference between the particle surface and the fluid, heat is transferred from the particle to the fluid. It should be noted that the heat transfer rate along the particle surface depends on the position on the surface, as a result of different fluid velocities along the surface, which are a function of angle of the stagnation point.

In common engineering practice, the particle-to-fluid heat transfer is expressed by the following model:

$$\bar{h} = \frac{\bar{q}''}{T_s - T_\infty} = \frac{q}{\pi d_p^2 (T_s - T_\infty)} \tag{3}$$

The average Nusselt number of a single sphere is

$$\overline{Nu} \equiv \frac{\bar{h} d_p}{\lambda} = \frac{\bar{q}}{\pi d_p \lambda \, \Delta T} \tag{4}$$

This model works well for simple cases, like a single free sphere, where the temperature difference between the surface and bulk temperature is well defined. However, it is less applicable to channels, packed beds or the CSP, because the bulk temperature is not easily defined. Therefore, in our study the temperature difference in the CSP, or a channel packed with particles, between the particle surface and the bulk is based on the average of the mass averaged temperatures of the fluid at the cross-section perpendicular to the main flow direction of the channel, just upstream and downstream of the section of the channel that contains the 'warm', heat transferring, particle:

$$\Delta T = T_s - \tfrac{1}{2} T|_{in} - T|_{out} \tag{5}$$

This definition works well if the temperature difference $T|_{in} - T|_{out}$ is small compared to the driving force defined in Eq. (5). This ratio depends on conditions (mainly Reynolds and $a = \lambda / \rho C_p$), which to some extent can be freely chosen. As a result, the Nusselt numbers, obtained via simulation, will be less accurate at low than at high Reynolds numbers.

2.2. Heat transfer for a single free sphere and spheres packed in channel

First, a benchmark for the simulation of the heat transfer rate of a single free sphere in an 'infinite' flowing medium will be carried out. The Reynolds number for this benchmark is defined as

$$Re \equiv \frac{\rho v_\infty d}{\mu} \tag{6}$$

The benchmark heat transfer simulations will be compared to the empirical heat transfer relations by Ranz and Marshall [17], Whitaker [23] and Achenbach [1] for a single free sphere, respectively:

$$Nu = 2.0 + 0.66 Re^{0.5} Pr^{0.33}, \quad \text{for } 10 < Re < 10^4, Pr > 0.7, Pe \gg 1 \tag{7}$$

$$Nu = 2.0 + (0.4 Re^{0.5} + 0.06 Re^{0.67}) Pr^{0.4}, \quad \text{for } 3.5 < Re < 7.6 \times 10^4, 0.7 < Pr < 380 \tag{8}$$

$$Nu = 2.0 + \left(\tfrac{1}{4} Re + 3 \times 10^{-4} Re^{1.6} \right), \quad \text{for } 10^2 < Re < 2 \times 10^5 \tag{9}$$

Second, the particle-to-fluid heat transfer in a single CSP channel, i.e., a narrow channel packed with particles, will be simulated. The conventional engineering relation for heat transfer in a randomly packed bed is

$$Nu = (1.8 \pm 0.3) Re^{0.5} Pr^{0.33}, \quad \text{for } \epsilon = 0.4, 30 < Re < 3 \times 10^3, Pr \geq 1 \tag{10}$$

Note that in this conventional engineering equation the limiting value of Nusselt (i.e. the constant c_1 in Eq. (1)) is generally dropped [7,19]. For the modelling of flow in a single CSP channel, a channel flow approach is preferred, as this worked well for pressure drop modelling [4]. In this approach, the Reynolds number for the CSP is based on the

interstitial velocity (v_i) and the hydraulic diameter (d_H) of the CSP-channel:

$$Re_H \equiv \frac{\rho v_i d_H}{\mu} \tag{11}$$

where the hydraulic diameter and interstitial velocity are defined as

$$\langle d_H \rangle \equiv \frac{4V_{gas}}{A_w + A_p} = \frac{4\epsilon}{6(1-\epsilon) + (4/N)} d_p \tag{12}$$

$$v_i \equiv \frac{v_s}{\epsilon} \tag{13}$$

The Reynolds number based on the hydraulic diameter is implemented in the heat transfer correlation for randomly packed beds (Eq.(10)), to be able to apply this correlation properly to the CSP, which results in

$$Nu = (2.7 \pm 0.5) Re^{0.5} Pr^{0.33}, \quad \text{for } \epsilon = 0.4,\ 20 < Re < 2 \times 10^3,\ Pr \geq 1 \tag{14}$$

2.3. Experimental determination of the mass transfer characteristics

Mass transfer is characterized by the Sherwood number:

$$Sh \equiv \frac{k_g d_p}{D} \tag{15}$$

In our work, the particle-to-fluid mass transfer characteristics of the CSP (or more general: narrow channels filled with particles) are investigated using the naphthalene sublimation technique with spherical naphthalene particles. The molar flow rate of the naphthalene from the particle surface to the bulk gas is expressed as

$$\varphi_{mol} = \frac{\Delta m}{M\, \Delta t} = k_g \pi \langle d_p \rangle^2 \left(C_s - C_{s,bulk}\right) \tag{16}$$

where Δm is the mass decrease of the naphthalene sphere during time Δt of an experiment. The naphthalene concentration at the surface of the naphthalene particle is given by:

$$C_s \equiv \frac{n}{V} = \frac{P^{sat}}{RT} \tag{17}$$

where the saturated vapor pressure is estimated with the temperature dependent correlation of Ambrose et al. [2], recommended by Goldstein and Cho [10]. In our experiments, the conditions are chosen such that the concentration in the bulk of the gas phase (i.e. the mixing cup average) remains below 5% of the saturation value and can therefore be assumed zero within an acceptable error margin. Eq. (16) can then be rewritten as

$$k_{g,experimental} = \frac{\Delta m}{\pi \langle d_p \rangle^2 C_s M_s\, \Delta t} \tag{18}$$

in which the mass decrease of the sphere must be determined experimentally. Finally the Schmidt number is estimated from Cho and the diffusion coefficient of naphthalene in air is estimated from the average of the value of Cho and of Chen and Wung as recommended by Goldstein and Cho [10].

To relate the heat transfer simulations to the mass transfer experiments, the Chilton–Colburn analogy is applied. In this analogy, the heat transfer number j_H and the mass transfer number j_D are defined as

$$j_H \equiv \frac{Nu}{RePr^{1/3}} \quad \text{and} \quad j_D \equiv \frac{Nu}{ShSc^{1/3}} \tag{19}$$

For geometrical similarity j_H equals j_D. In this way, the mass transfer experiments can be used to validate the CFD heat transfer simulations.

3. CFD modelling

3.1. Heat transfer from single free sphere to fluid

A solid sphere of 12.7 mm diameter, with a temperature of 310 K, was defined in a cylindrical domain, which had 'open' boundary conditions to simulate an 'infinite' domain, with uniform static pressure boundary function. In this work, the domain sizes are expressed in parameters a, b and c, which are multiples of the sphere diameter, as shown in Fig. 2. Cases with parameters $[a, b, c]$ equal to [1.5, 5.5, 5], [4.5, 8.5, 10] and [9, 17, 20] were simulated. For a similar case, Mansoorzadeh et al. [15] used a domain size of [5, 20, 5]. The fluid was defined to be incompressible; the stationary situation was considered. The fluid entered the domain inlet with a temperature of 300 K, consequently being heated by the sphere. CFD modelling was done in CFX-5.3 from AEA Technology. An unstructured grid was used. Laminar simulations were done for $1.27 \times 10^{-4} < Re < 127$ and turbulent simulations for $127 < Re < 1.27 \times 10^5$. The k–ϵ, the RNG k–ϵ and the Reynolds Stress turbulence models were used. In laminar flow, steep radial temperature profiles occurred close to the surface of the sphere. At low Reynolds numbers, the temperature profile extends through a considerable part of the domain (i.e. over several particle diameters). Consequently, a fine mesh is required close to the surface of the sphere, whereas a somewhat coarser mesh is allowed further away from the surface. This was resolved by using a mesh inflation at the sphere surface, i.e., five thin layers of prismatic cells, with a thickness that increases per layer in the radial direction. For solutions that were sufficiently grid independent, up to 1.6×10^6 mesh cells were required, with the first layer of cells having a thickness of 1.8×10^{-4} times the sphere diameter. In turbulent flow, the laminar sub-layer and buffer layer were described by standard wall functions in the first layer of mesh cells around the sphere. Thus, the steep gradients close to the sphere surface were modelled in a single layer of grid cells. As a result, somewhat less mesh cells were required (up to 2.5×10^5) than for laminar flow. The results are presented in Fig. 3.

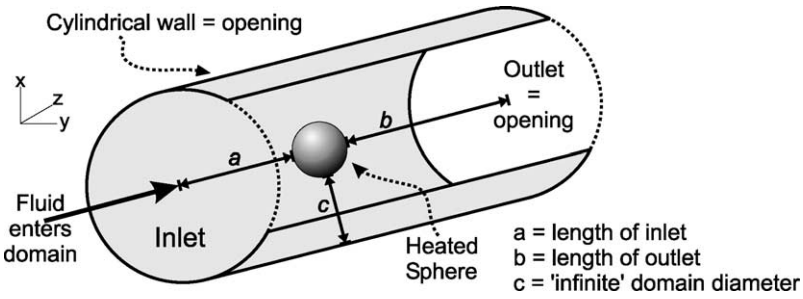

Fig. 2. Benchmark geometry.

The heat transfer rate is predicted within an error of 5% for $1 < Re < 10^3$, depending on the literature that is chosen for comparison [17,23]. For $10^3 < Re < 10^5$ the model shows prediction within an error of 10% (in between Whitaker [23] and Achenbach [1]). Second-order discretisation schemes gave better predictions than the first-order scheme. It was found that heat transfer predictions deviated considerably from theory if Reynolds was varied by changing the viscosity at constant fluid density and velocity, resulting in high Prandtl numbers (up to 10^5). It proved that simulations should be carried out for $Pr \gtrapprox 1$ in order not to obtain erroneous heat transfer predictions. Hence, it was decided to use the density to set the Reynolds number and to keep Prandtl fixed at unity. No significant influence on the heat transfer rate of the fluid domain size was found between the factor 10 or 20 for parameter c in Fig. 2.

It was found that the RNG k–ϵ model gave heat transfer predictions that were somewhat better in the range of the experimental data, than the more widely used k–ϵ model. This can be explained by the limited performance of the k–ϵ model on curved boundary layers [21]. Simulations with the Reynolds Stress turbulence model gave similar predictions to RNG k–ϵ models, which does not justify the higher computing effort of the latter.

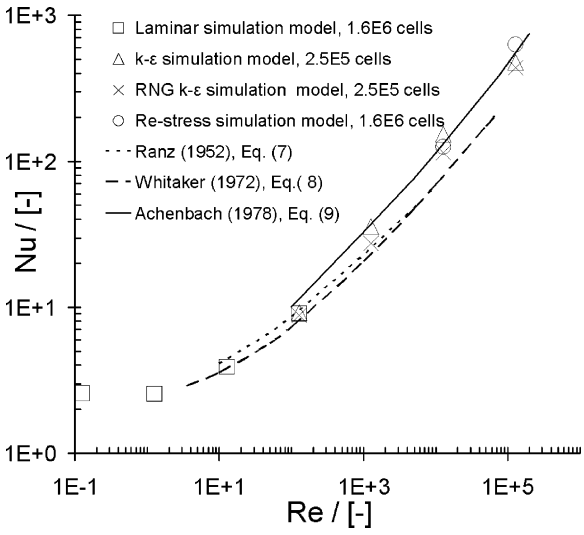

Fig. 3. Heat transfer for a single free sphere; Nusselt vs. Reynolds.

The non-dimensional parameter y^+ is used to verify the mesh adequacy for turbulent simulations. This parameter is used to determine the dimensionless thickness of the wall cell and depends on the mesh size in the wall region. If the value of y^+ is too large, the wall function will impose the wall type condition further from the wall than is physically appropriate. Conversely, a too small value means the spanning of a too small portion of the physical boundary layer, which is also physically inappropriate. A typical value for y^+ between 30 and 300, or at least between 10 and 1000, is generally recommended for best accuracy.

In the present study, the y^+ criterion was only met at the higher Reynolds numbers. At the lower Reynolds numbers, y^+ values even smaller than 1 were obtained, even with meshes that could be considered coarse with respect to discretisation errors. The good results that were nevertheless obtained, indicate that the CFX code is apparently quite robust outside the recommended range of y^+.

It is well known that in the single free sphere model the fluid velocity as well as the particle-to-fluid heat transfer (or local Nusselt number) along the sphere surface are a function of the angle relative to the stagnation point. This phenomenon is also reported by Lloyd and Boehm [14] in 2D CFD simulations of flow and heat transfer around spheres, as well as by Giedt [8] for circular cylinders in cross flow. The heat transfer at different Reynolds numbers as a function of the angle relative to the stagnation point are plotted in Figs. 4 and 5. In Fig. 6, detailed flow profiles and heat transfer plots are presented for three different Reynolds numbers. The results agree with the work of Giedt [8], and Lloyd and Boehm [14], although direct comparison with literature data is not possible.

3.2. Particle-to-fluid heat transfer in the CSP

In the CFD model of the CSP, the particle-to-fluid heat transfer was simulated by defining all solids (spheres, channel wall) to be adiabatic, except for one or more ‘active’ spheres, which were given a higher surface temperature than the inlet temperature of the fluid. The integral value of the resulting heat flux from the sphere to the fluid was used

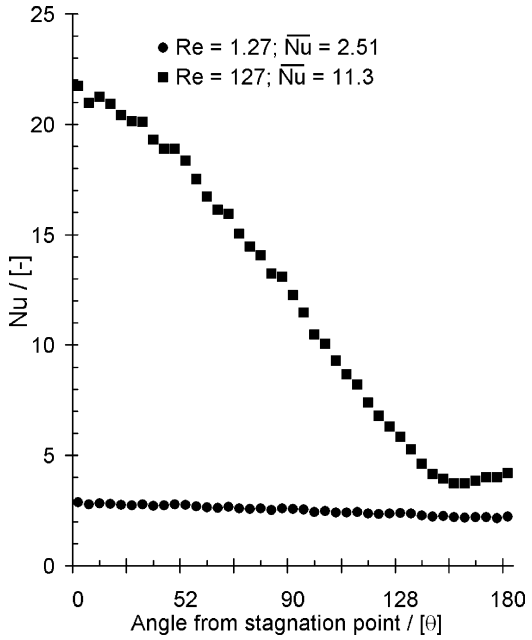

Fig. 4. Local Nusselt number as function of angle from stagnation point (θ) at low Reynolds.

for calculation of the particle average Nusselt number. The most important aspects of the CFD model are: single channel with square cross-section with 8–16 spherical particles, shrunken particle diameters (1%) to avoid grid generation problems because of solid contact points [4], unstructured grid with prismatic cells in the first five mesh layers from the solid surfaces and tetrahedral cells in the remaining

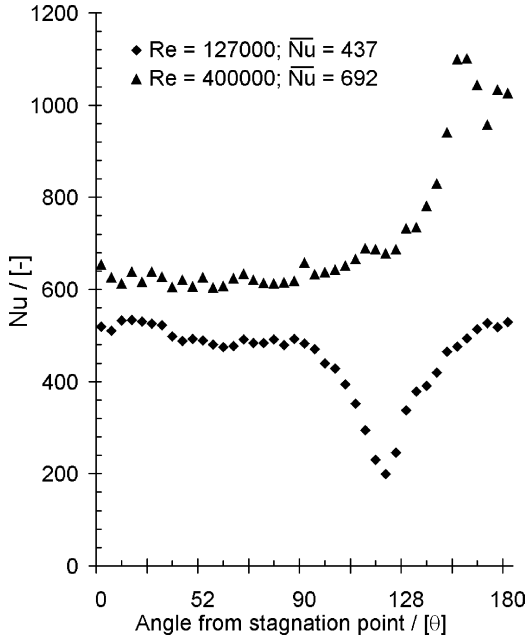

Fig. 5. Local Nusselt number as function of angle from stagnation point (θ) at high Reynolds.

volume, incompressible flow that was assumed to be stationary, Reynolds number (based on interstitial velocity and hydraulic diameter) ranging from 10^{-2} to 10^{5}, k–ϵ and RNG k–ϵ turbulence models, standard wall functions in the case of turbulent flow.

Five CSP geometries were simulated. Ducts with a square cross-section were filled with arrays of 8–16 particles, depending on the channel-to-particle-diameter ratio. These geometries are identical to the ones used in the dimensions of the mass transfer experiment setup (see Fig. 1), except for the length of the packing. The number of spheres and the channel length are limited because longer channels would increase the number of mesh cells needed, which is limited by computing resources. It was shown in previous pressure drop CFD simulations by Calis et al. [4] that even the short packings, containing only 8–16 particles, represent the characteristics of the CSP adequately, as far as flow profile and pressure drop are concerned.

The ‘active’ spheres were given a fixed temperature (rather than a fixed heat flux) because a constant surface temperature in the heat transfer simulations resembles the boundary condition in the naphthalene mass transfer experiments (i.e. a constant surface concentration). The Nusselt number is based on the integral heat transfer rate over the complete sphere, although it is obvious that the heat flux is not uniform, as is illustrated by the CFD simulation (see Fig. 7).

Various aspects of the simulation model were investigated in order to assess the validity of the simulated heat transfer rates. Different mesh sizes were tested, different shrink factors, the influence of the position and the number of ‘active’ spheres, before finally all five different channel-to-particle-diameter ratios were simulated.

To obtain a heat transfer rate that showed to approach grid size independency, the grid cell thickness at the (heated) sphere surfaces needed to be about 17 μm (compared to a particle diameter of 12.7 mm), in grids with up to 3.4 million cells for laminar flow. Turbulent flow posed the dilemma that a fine mesh is needed to limit discretisation errors, which conflicts with the constraint of the y^+ value that sets a lower limit to the wall (grid) cell size. It was found that the heat transfer with CFX is only weakly dependent on the y^+ values between 0.1 and 1000. Mass/enthalpy balance residuals were on average lower than 0.05%.

In order not to generate solid–solid contact points to prevent mesh generation problems, the spheres were shrunk by 1% after determining the positions of the spheres in the channel [4]. The influence of this shrink factor on the heat transfer and fluid velocity was investigated by comparing with shrink factors of 2, 3 and 5% after correcting Reynolds for the increased porosity. From these simulations, it was found that the heat transfer for a shrink factor of 1% is representative (<5% relative error) for the full solid–solid contact, which agrees with the work of Nijemeisland and Dixon [16] on channel-to-fluid heat transfer. They used a similar approach in their so-called ‘near-miss’ model.

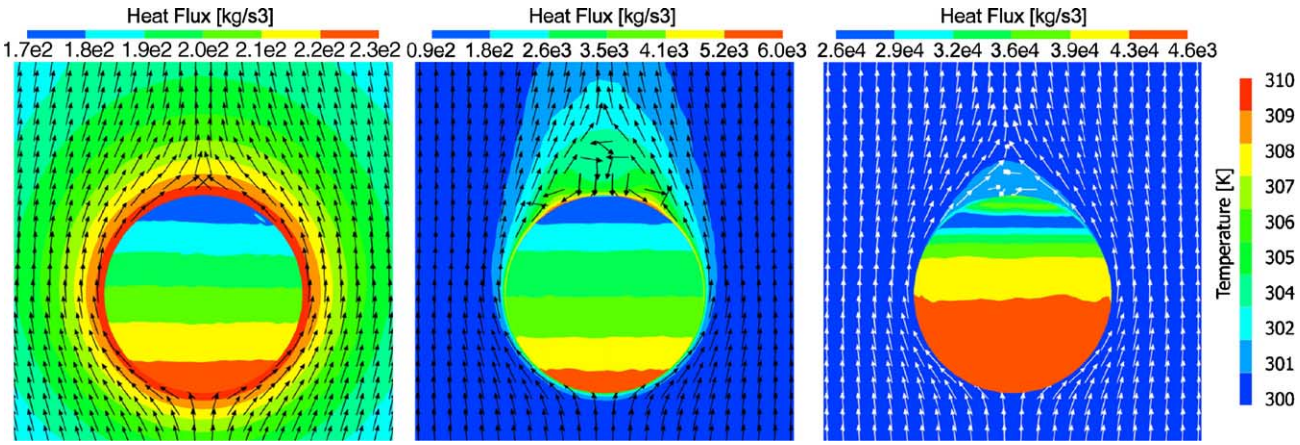

Fig. 6. Cross-section of a small part of the total fluid domain of the benchmark. The flow direction is represented by the vectors around the sphere. Two color scales are available; the heat flux scale is valid for the circular sphere surface, whereas the temperature scale is valid for the fluid domain. They pertain to (a) $Re = 1.27$, (b) $Re = 127$ and (c) $Re = 127000$.

The influence of the number and position of the 'active' particles on the Nusselt number was investigated. It was found that in the packing of $N = 1.00$, the third to the seventh particle (the packing contained eight particles) are representative for the heat transfer, i.e. the same Nusselt number is found for each position (<3% relative error). This indicates that the flow becomes periodic with respect to the heat transfer after the second particle. The flow is not yet periodic in the region of the first two particles, whereas back mixing effects at the rear end/outlet of the packing affect the heat transfer of the last particle. The Nusselt numbers were not affected (<3% relative error) by the number of 'active' particles in a row, provided, of course, that the correct bulk fluid temperatures were used for each 'active' particle in the calculation of the heat transfer coefficient from the total heat flux of a particle (see Section 2.1, Eq. (5)). This shows that the approach, explained in Section 2.1 is correct. Only at low Reynolds numbers ($Re < 10$), in case of multiple heated particles, it was found that the Nusselt numbers for the different particles in a row were not equal. This effect is attributed to the strongly decreasing temperature gradient between the particle and the fluid downstream, as a result of the heating of the bulk fluid in a row of heated particles. In the case of an almost stagnant fluid in a constrained space, the concept of the heat transfer coefficient starts breaking down (see Section 2.1). Similar tests were carried out for the packings with $N = 1.15$, 1.47, 2.00A and 2.00B, all showing the same packing inlet and outlet effects.

For packing 2.00B, two cases need to be discerned. Due to the geometry of the packing (see Fig. 1), from a flow profile and heat transfer point of view, two different particles can be distinguished: a particle in the centre (of the square cross-section) of the channel, with a layer of four particles both upstream and downstream, and a particle in one of

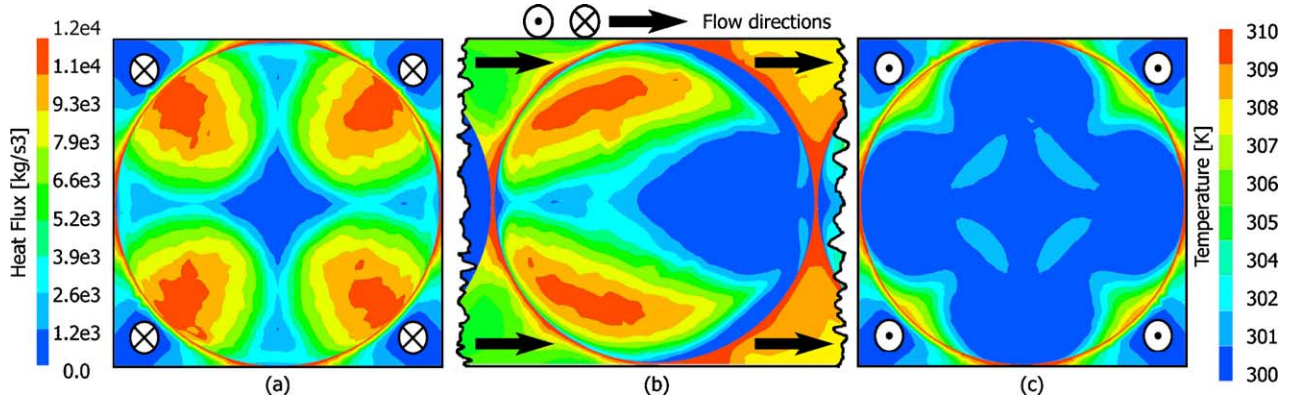

Fig. 7. Local heat transfer ($Re = 502$) over the surface of particle no. 3 in a linear array of spheres for $N = 1.00$, in front (a), side (b) and rear (c) view. Two color scales are available; the heat flux scale ($\mathrm{W\,m^{-2}} = \mathrm{kg\,s^{-3}}$)is valid for the sphere surface, whereas the temperature scale is valid for the fluid domain. It is clear that the heat transfer rate is lower in the stagnant zone, in the shade of the particle that is located upstream of the 'active' particle. The heat transfer rate at the downstream side of the 'active' particle is lower because of the stagnant zone and increased fluid temperature which causes a smaller temperature gradient between the local particle surface and fluid. The highest heat transfer rate is achieved on the side parts of the particle where the fluid has its highest velocity (lowest temperature) because of the square channel cross-section.

these layers of four, located in the corner of two walls (of the square cross-section). It was found that the Nusselt value of the centre particle was maximally 10% lower than the Nusselt value of the particles in a layer of four.

4. Experimental

The experimental values of the Sherwood numbers were obtained by replacing one or more spheres in the packing by spheres made of naphthalene, and determining the rate of mass decrease of the naphthalene spheres at constant gas velocity (Fig. 8).

Single channels made of PMMA walls were used, with square cross-sections of 12.7 to 26.0 mm, and a length of 700 mm [4]. High-precision plastic PE spheres of 12.7 mm diameter were supported by a screen. The inlet region of the channels contained a bed of 2 mm glass beads followed by a 400 csi monolith, to obtain a flat inlet velocity profile. High-precision naphthalene spheres of 12.7 mm diameter were prepared by gluing together two hemispheres, that were made by compressing the right amount of powdered naphthalene crystals in a hemispherical mould, such that a particle density of 1145 kg m^{-3} was obtained.

Upstream of the column, the flow was heated to 25 °C in order to obtain a sufficiently high mass transfer rate of naphthalene. The mass transfer rate was determined by weighing the naphthalene sphere right before and right after a run at a constant gas velocity. Experiments were carried out for packings with channel-to-particle-diameter ratios of 1.00, 1.47, 2.00*A* and 2.00*B* (see Fig. 1). The Reynolds number regimes were 300–4656, 210–6195, 101–2530 and 484–2251, respectively. A typical run was stopped before a 5% decrease of the mass of a particle occurred (corresponding to 1.7% diameter decrease), in order not to influence the flow profile and mass transfer rate in the CSP because of the decrease of the particle diameter. Measurements were done on the systemic error of mass decrease during the loading and unloading of the particle, which is corrected for in the calculation of the experimental Sherwood number. The resulting Sherwood numbers are plotted in Figs. 9–12, together with the Nusselt numbers obtained via CFD simulation.

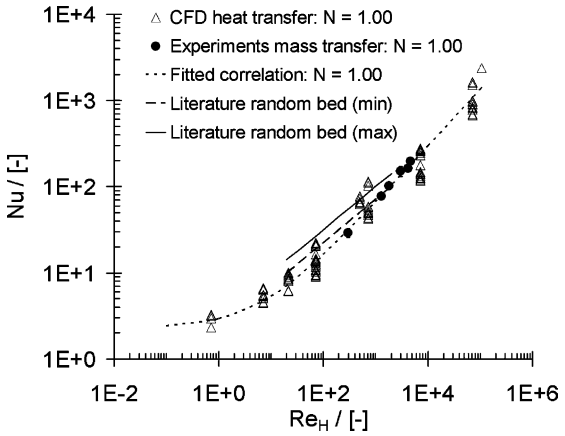

Fig. 8. Plot of simulated Nusselt numbers, experimental Sherwood numbers and fitted correlation vs. Reynolds numbers, $N = 1.00$.

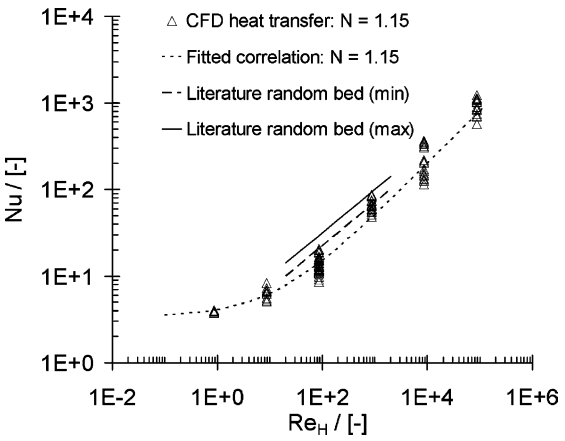

Fig. 9. Plot of simulated Nusselt numbers, experimental Sherwood numbers and fitted correlation vs. Reynolds numbers, $N = 1.15$.

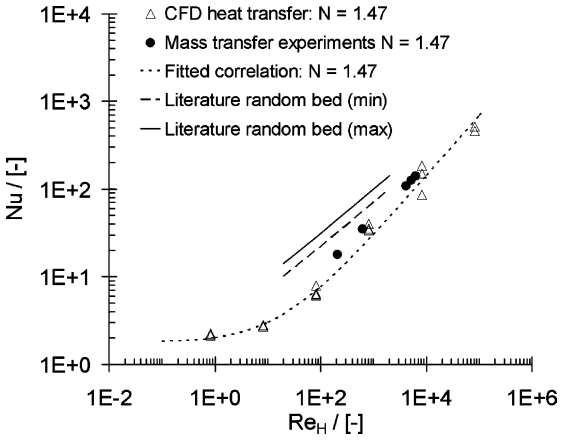

Fig. 10. Plot of simulated Nusselt numbers, experimental Sherwood numbers and fitted correlation vs. Reynolds numbers, $N = 1.47$.

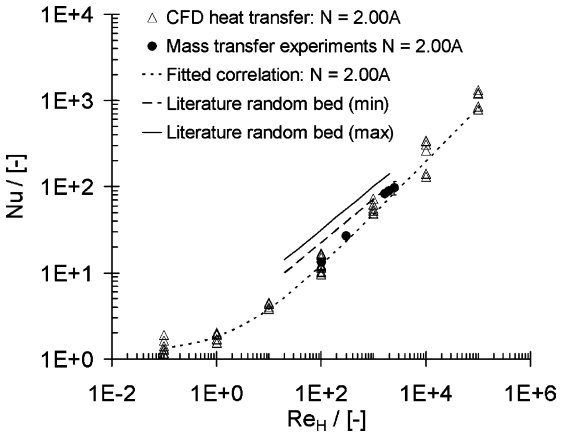

Fig. 11. Plot of simulated Nusselt numbers, experimental Sherwood numbers and fitted correlation vs. Reynolds numbers, $N = 2.00$A.

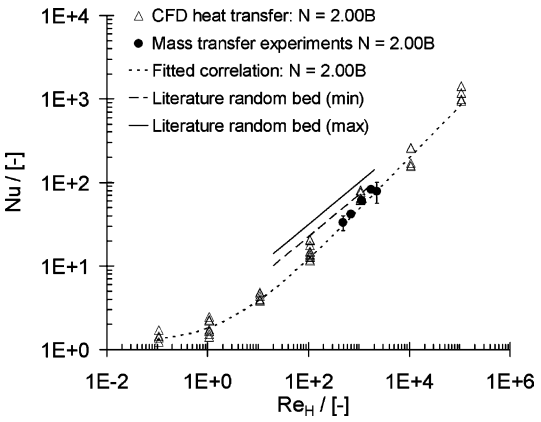

Fig. 12. Plot of simulated Nusselt numbers, experimental Sherwood numbers and fitted correlation vs. Reynolds numbers, $N = 2.00$B.

5. Validation

The simulated Nusselt numbers could be adequately fitted to the commonly used engineering correlation $Nu = c_1 + c_2 Re^n Pr^{1/3}$. These correlations pertain to the constant temperature boundary condition. Six correlations are developed, one for each specific channel-to-particle-diameter ratio and one generic correlation for square cross-section channels with $N \leq 2.00$. The fitted constants are listed in Table 1.

The constants are based on all heat transfer simulation results (coarse and fine meshes), which were reliable based on y^+ and ΔT criteria (Eq. (5)). The adequacy of the different engineering correlations compared to the individual simulation results is listed in Table 2 as a prediction error percentage. The error percentage was defined by comparing the predicted Nusselt values of the correlations, at the Reynolds numbers for which the experiments were carried out, and the mean value of the corresponding experimental Sherwood numbers, in the following way:

$$\text{error} = \frac{\sum_{i=1}^{x} \left| \left(Nu|^{Pr=1}_{\text{correlation}} / \left(\sum_{i=1}^{p} Sh|^{Sc=1}_{\text{experimental}} / p \right) - 1 \right) \times 100\% \right|}{x} \quad (20)$$

where x is the number of mass transfer experiments at different Reynolds numbers within the regimes described above, and p the total number of mass transfer experiments at a specific Reynolds number. The N-specific CFD correlations agreed well with the experimental Sherwood numbers: the deviations were less than 15%, except for $N = 1.47$ (which was 31%, attributed to the high voidage [4]). These results indicate that the CFD model can be used to develop acceptable specific and generic engineering correlations needed for the design of CSPs. The considerable deviation of the commonly used randomly packed bed model confirms that the packed beds with low N are 'special' cases.

Table 1
Fitted constants, based on CFD simulations, for the engineering correlations of Eqs. (1) and (2)

N	Parameters with 95% confidence interval		
	c_1	c_2	n
1.00	2.27 ± 0.62	0.67 ± 0.2	0.661 ± 0.038
1.15	3.33 ± 0.58	0.724 ± 0.0186	0.609 ± 0.030
1.47	1.77 ± 0.28	0.249 ± 0.058	0.688 ± 0.026
2.00A	1.16 ± 0.2	0.629 ± 0.130	0.623 ± 0.026
2.00B	0.872 ± 0.164	0.770 ± 0.112	0.624 ± 0.018
≤2.00	1.06 ± 0.2	0.796 ± 0.124	0.621 ± 0.02

Table 2
Prediction error percentages of different engineering correlations

N	N-specific CFD correlation (%)	Generic CFD correlation, $N \leq 2.00$ (%)	Randomly packed bed correlation (Eq. (14)) (%)
1.00	6	15	19
1.47	31	29	75
2.00A	15	7	58
2.00B	10	11	60

6. Conclusions

Commercial CFD software can be used to adequately predict the particle-to-fluid heat transfer of a single free sphere as well as particles in a square channel packed bed with low ($1.00 \leqslant N \leqslant 2.00$) channel-to-particle-diameter ratio. These predictions can be used to develop simple reactor engineering correlations, which predict the mass and heat transfer rate within an average error of 15% for Reynolds numbers ranging from 10^{-1} to 10^5. The good agreement between simulated and experimental results gives confidence in the application of CFD simulation to predict the characteristics of fixed beds, or packings in general.

The required number of grid cells is at the limit of today's acceptable computing power. It is anticipated however, that within a few years, computer power and CFD modelling will have advanced to a point where simulation of heat/mass transfer in packed beds up to a few hundred particles, is considered a 'standard problem'.

Acknowledgements

The authors would like to thank the ABB Corporate Research Center//Alstom Power in Switzerland for their hospitality to the last author during part of the modelling study.

References

[1] E. Achenbach, in: Proceedings of the 6th International Heat Transfer Conference on Heat Transfer from Spheres up to $Re = 6 \times 10^6$, vol. 5, Hemisphere, Washington, DC, 1978.
[2] D. Ambrose, I.J. Lawrenson, C.H.S. Sparke, The vapor pressure of naphthalene, J. Chem. Ther. 7 (1975) 1173–1176.

[3] R.B. Bird, W.E. Stewart, E.N. Lightfoot, Transport Phenomena, first ed., Wiley, New York, 1960.
[4] H.P.A. Calis, J. Nijenhuis, B. Paikert, F.M. Dautzenberg, C.M. Va den, CFD modelling and experimental validation of pressure drop and flow profile in a novel structured catalyst packing, Chem. Eng. Sci. 56 (2001) 1713–1720.
[5] M.T. Dalman, J.H. Merkin, C. McGreavy, Fluid flow and heat transfer past two spheres in a cylindrical tube, Comput. Fluids 14 (3) (1986) 267–281.
[6] O.R. Derkx, A.G. Dixon, Determination of the fixed bed wall heat transfer coefficient using Computational Fluid Dynamics, Num. Heat Trans., Part A 29 (1996) 777–794.
[7] E.R.G. Eckert, Trans. ASME 56 (1956) 1273–1283.
[8] W.H. Giedt, Investigation of variation point unit-heat-transfer around a cylinder normal to an air stream, Trans. ASME 71 (1949) 375–381.
[9] V. Gnielinski, Gleichungen zur Berechnung des Wärme- und Stoffaustausches in durchströmten ruhenden Kugelschüttungen bei mittleren und großen Pécletzahlen, vt-Verfahrenstechnik 12 (1978) 363–366.
[10] R.J. Goldstein, H.H. Cho, A review of mass-transfer measurements using naphthalene sublimation, Exp. Therm. Fluid Sci. 10 (4) (1995) 416–434.
[11] S.A. Logtenberg, A.G. Dixon, Computational Fluid Dynamics studies of fixed bed heat transfer, Chem. Eng. Proc. 37 (1998) 7–21.
[12] S.A. Logtenberg, A.G. Dixon, Computational Fluid Dynamics studies of the effects of temperature-dependent physical properties on fixed bed heat transfer, Ind. Eng. Chem. Res. 37 (1998) 739–747.
[13] S.A. Logtenberg, M. Nijemeisland, A.G. Dixon, Computational Fluid Dynamics simulations of fluid flow and heat transfer at the wall-particle contact points in a fixed bed reactor, Chem. Eng. Sci. 54 (1999) 2433–2439.
[14] B. Lloyd, R. Boehm, Flow and heat transfer around a linear array of spheres, Num. Heat Trans., Part A 26 (1994) 237–252.
[15] S. Mansoorzadeh, C.C. Pain, C.R.E. De Oliviera, Finite element simulations of incompressible flow past a heated/cooled sphere, Int. J. Num. Methods Fluids 28 (1998) 903–915.
[16] M. Nijemeisland, A.G. Dixon, Comparison of CFD simulations to experiment for convective heat transfer in a gas-solid fixed bed, Chem. Eng. J. 82 (Special) (2001) 231–246.
[17] W.E. Ranz, W.R. Marshall, Evaporation from drops, Chem. Eng. Prog. 48 (Part I) (1952) 141–146.
[18] V.A. Strangio, F.M. Dautzenberg, H.P.A. Calis, A. Gupta, Fixed catalytic bed reactor, International Patent Application PCT/US99/06242, priority date 23 March 1998.
[19] D. Thoenes, H. Kramers, Chem. Eng. Sci. 8 (1958) 271.
[20] E. Tsotsas, E.U. Schlünder, Measurement of mass transfer between particles and gas in packed beds at very low tube to particle diameter ratios, Wärme- und Stoffübertrag 25 (1990) 245–256.
[21] H.K. Versteeg, W. Malalasekera, An Introduction to Computational Fluid Dynamics, The Finite Volume Method, Addison Wesley, Harlow, 1995, p. 74.
[22] N. Wakao, T. Funazkri, Effect of fluid dispersion coefficients on particle-to-fluid mass transfer coefficients in packed beds: correlation of Sherwood numbers, Chem. Eng. Sci. 33 (1978) 1375–1384.
[23] S. Whitaker, Forced convection heat transfer correlations for flow in pipes, past flat plates, single cylinders, single spheres, and for flow in packed beds and tube bundles, AIChE J. 18 (1972) 361–371.
[24] M. Winterberg, E. Tsotsas, Modelling of heat transport in beds packed with spherical particles for various bed geometries and/or thermal boundary conditions, Int. J. Ther. Sci. 39 (1999) 556–570.
[25] M. Winterberg, E. Tsotsas, Correlations for effective heat transport coefficients in beds packed with cylindrical particles, Chem. Eng. Sci. 55 (2000) 5937–5943.
[26] M. Winterberg, E. Tsotsas, Impact of tube-to-particle-diameter ratio on pressure drop in packed beds, AIChE J. 46 (5) (2000) 1084–1088.